Diffraction from diffusion-barrier-induced mound structures in epitaxial growth fronts

Y.-P. Zhao
Department of Physics, Applied Physics, and Astronomy, and Center for Integrated Electronics and Electronics Manufacturing, Rensselaer Polytechnic Institute, Troy, New York 12180-3590

H.-N. Yang
Department of Physics, Applied Physics, and Astronomy, and Center for Integrated Electronics and Electronics Manufacturing, Rensselaer Polytechnic Institute, Troy, New York 12180-3590 and Sharp Microelectronics Technology, Inc., Camas, Washington 98607

G.-C. Wang and T.-M. Lu
Department of Physics, Applied Physics, and Astronomy, and Center for Integrated Electronics and Electronics Manufacturing, Rensselaer Polytechnic Institute, Troy, New York 12180-3590

(Received 19 May 1997)

We construct models for the characteristic functions describing the mound structures induced by a surface diffusion barrier in epitaxial growth fronts. These characteristic functions, including the height-height correlation functions, are used to calculate the angular distribution of diffraction intensity. We compare in detail the characteristics of the reciprocal space structure for diffusion-barrier-induced and noise-induced roughening of epitaxial growth fronts. It is shown that except near the out-of-phase (anti-Bragg) diffraction condition, the reciprocal space structure of the diffusion-barrier-induced growth front contains splitting (ring) and broadening characteristics that are dramatically different from that obtained from a scale invariant growth front caused by random noises that exist during growth. This result allows us to differentiate unambiguously, using diffraction techniques, the two mechanisms that can cause the roughening of expitaxial growth fronts.
[S0163-1829(98)01403-9]

I. INTRODUCTION

Study of epitaxial growth of a material onto a crystalline substrate in vacuum is one of the most intriguing ventures for researchers in the last few decades from both a basic science and a technological point of view. The lattice constant of the depositing material and the substrate may not always be the same. Homoepitaxy refers to the class of systems where the depositing material and substrate are the same so that there is no lattice mismatch between them. Therefore, in principle one would expect the growth front to be perfectly smooth and free of defects provided that the surface of the substrate is defect-free to begin with. This indeed can happen. Within a certain temperature regime, the growth is layer-by-layer in which the incoming atoms would diffuse on the surface and would completely cover the surface before they start the next layer.[1] However, this does not happen all the time. In fact, the growth front can be rough in that multilayer step structures can occur during growth.[2–4]

Two mechanisms have been proposed to explain the roughening of the growth front in homoepitaxy. The first mechanism is related to the asymmetric diffusion barrier (Schwoebel barrier) that exists at surface steps, which inhibit a down-hill flow of atoms during growth. As a result, large structures in the form of ''mounds'' are created due to this Schwoebel barrier (SB) mechanism.[3] The other mechanism has to do with the random noise that exists during growth.[4] A fractal-like (self-affine) structure is created that possesses a scaling in space and time. Imaging techniques such as scanning tunneling microscopy with atomic resolution (so that the step structure can be observed) has been particularly powerful in identifying the nature of the roughening.[5] Diffraction technique,[6] on the other hand, is very powerful in obtaining the statistical values of the growth parameters over a large area in a short time.

Recent calculations for the self-affine surface indicated that in the scaling regime, the diffraction beam obtained at the out-of-phase, or anti-Bragg condition, is a single broadened peak.[7] This profile looks very similar to that obtained from a mound surface caused by the SB effect as the interface width grows sufficiently large.[8,9] The well established wavelength selection in the mound formation unfortunately does not result in beam splitting in diffraction under the out-of-phase diffraction condition when the interface width becomes sufficiently large. The similarity in the diffraction profiles obtained from the self-affine and mound surfaces causes difficulty in the distinction of the two mechanisms and also, prevents one to obtain quantitative information of the growth front.

In this paper, we show that if one moves away from the out-of-phase diffraction condition, the general reciprocal space structure obtained from a self-affine rough surface is dramatically different from that obtained from a rough mound surface caused by the SB effect. Specifically at the near in-phase diffraction condition, the SB effect always gives a clear ring diffraction structure for the mound formation. Quantitative information such as average mound separation, lateral correlation length, and the interface width can be extracted from the reciprocal space structure. This ring structure does not exist in the case of the self-affine rough surface. We also include a discussion of specific models that lead to the characteristic height-height correlation functions

for both noise-induced and SB-induced rough growth fronts.

The organization of the paper is as follows: in Sec. II we describe the different characteristics of surface morphology for both the noise-induced mechanism and the Schwoebel barrier effect through the solution of continuous Langevin equations. To catch the essence of those solutions and to simplify the diffraction calculations, we propose some model functions to differentiate the surfaces caused by these two mechanisms in Sec. III, along with their properties. In Sec. IV we present the detailed reciprocal space structures for the proposed characteristic functions. We end the paper with a comparison of our model with a mound surface, discussions, and conclusion remarks.

II. MODELS FOR GROWTH FRONT ROUGHENING

In order to compare the reciprocal space structures for different roughening mechanisms, we need to understand the main features of rough surfaces in real space. This can be achieved by studying the characteristic functions of the surfaces. Different characteristic functions, such as height-height correlation function $H(\mathbf{r})$, autocorrelation function $R(\mathbf{r})$, and power spectrum $P(\mathbf{q})$, have been used to describe the rough surfaces. These three functions are related, and their definitions and relations are given by

$$R(\mathbf{r})=\langle h(\mathbf{r})h(0)\rangle, \tag{1a}$$

$$H(\mathbf{r})=\langle[h(\mathbf{r})-h(0)]^2\rangle=2[w^2-R(\mathbf{r})], \tag{1b}$$

$$P(\mathbf{q})=\frac{1}{(2\pi)^{d/2}}\int R(\mathbf{r})e^{-i\mathbf{q}\cdot\mathbf{r}}d\mathbf{r}. \tag{1c}$$

Here $h(\mathbf{r})$ is the surface height at position $\mathbf{r}$ on the surface, $w=\sqrt{\langle[h(\mathbf{r})-\bar{h}]^2\rangle}$ is called the interface width, and $\bar{h}$ is the average surface height. The difference between $H(\mathbf{r})/2$ and $R(\mathbf{r})$ is only a constant, while $P(\mathbf{q})$ and $R(\mathbf{r})$ are Fourier transform pairs. Using any of these three functions to describe a surface should give an equivalent result. In this section, we shall obtain the power spectra analytically from some simplified Langevin equations. More generally, in the next section, we shall give all three forms of the characteristic functions.

A. Noise-induced growth

In this model, the roughening is caused by the competition between the inherent thermal noise in the growth system and the smoothing effect by a condensation/evaporation process on the surface. Sometimes the capillary effect, i.e., Mullins diffusion, is also included. A simple linear Langevin equation including all these effects is given by[4]

$$\frac{\partial h(\mathbf{r},t)}{\partial t}=\nu\nabla^2 h-\kappa\nabla^4 h+\eta(\mathbf{r},t), \tag{2}$$

where ν is the surface tension, and κ is the Mullins diffusion coefficient. $\eta(\mathbf{r},t)$ is a Gaussian white noise, satisfying

$$\langle\eta(\mathbf{r},t)\rangle=0,$$

$$\langle\eta(\mathbf{r},t)\,\eta(\mathbf{r}',t')\rangle=2D\,\delta(\mathbf{r}-\mathbf{r}')\,\delta(t-t'). \tag{3}$$

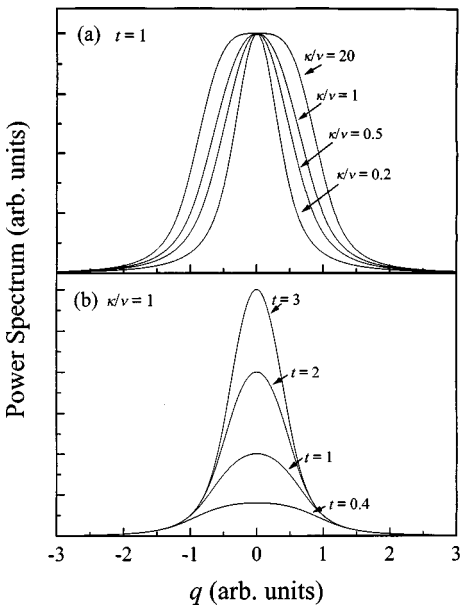

FIG. 1. The power spectrum of a noise-induced roughening front determined by Eq. (7). (a) κ/ν ratio-dependent (let $t=1$); (b) time-dependent (let $\kappa/\nu=1$).

The solution for Eq. (2) is simple and straightforward through a spatial Fourier transformation, given by the following expression:

$$h(\mathbf{r},t)=\left(\frac{1}{2\pi}\right)^{d/2}\int d\mathbf{q}\;e^{i\mathbf{q}\cdot\mathbf{r}}\int_0^t d\tau\;\Theta(\mathbf{q},\tau)e^{-(\kappa q^4+\nu q^2)(t-\tau)}, \tag{4}$$

where $\Theta(\mathbf{q},t)$ is the spatial Fourier transformation of $\eta(\mathbf{r},t)$,

$$\Theta(\mathbf{q},t)=\left(\frac{1}{2\pi}\right)^{d/2}\int d\mathbf{r}\;\eta(\mathbf{r},t)e^{-i\mathbf{q}\cdot\mathbf{r}} \tag{5}$$

and

$$\langle\Theta(\mathbf{q},t)\rangle=0,$$

$$\langle\Theta(\mathbf{q},t)\Theta(\mathbf{q}',t')\rangle=2D\,\delta(\mathbf{q}+\mathbf{q}')\,\delta(t-t'). \tag{6}$$

The power spectrum is given by

$$P(\mathbf{q})=4D\,\frac{1-e^{-2(\kappa q^4+\nu q^2)t}}{\kappa q^4+\nu q^2}. \tag{7}$$

A plot of the power spectrum with different κ/ν ratios and growth time t is shown in Fig. 1. The full width at half maximum (FWHM) of the power spectrum is determined by both the κ/ν ratio and deposition time t, and is a reflection of the lateral correlation length ξ. The interface width w and local slope m can be calculated from the power spectrum according to the following relations:[10]

$$w^2=\int P(\mathbf{q})d\mathbf{q}, \tag{8}$$

$$m^2=\int q^2P(\mathbf{q})d\mathbf{q}, \tag{9}$$

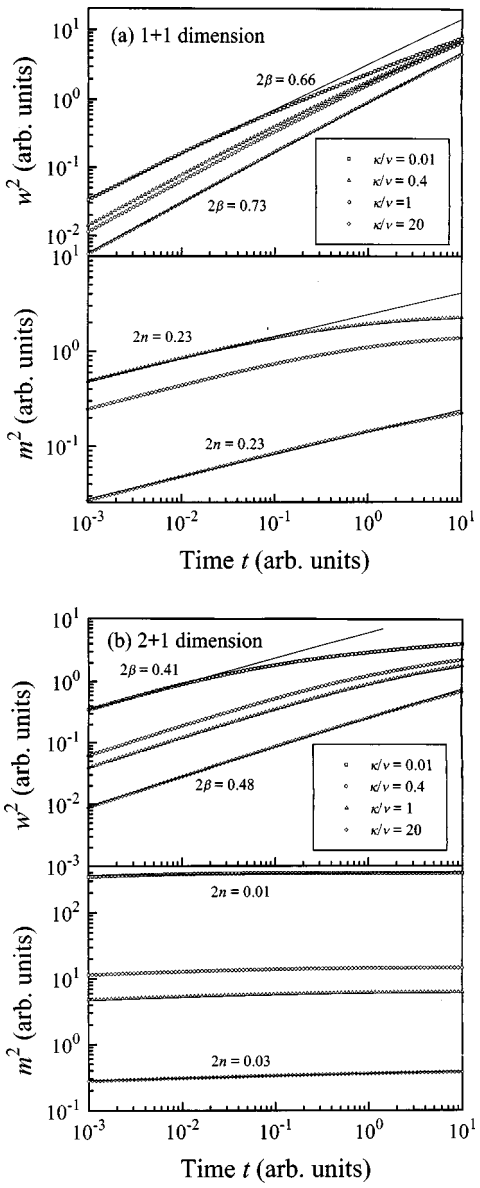

FIG. 2. Time evolution of the interface width w^2 and local slope m^2 of the noise-induced rough growth front. (a) $1+1$ dimension, and (b) $2+1$ dimension.

respectively. The numerical integration of interface w^2 and local slope m^2 for different κ/ν ratios are shown in Fig. 2 for $1+1$ and $2+1$ dimensions. We let $w \sim t^{\beta}$. As the Laplacian term is also a smoothing effect, the β value $[(2-d)/4 \leqslant \beta \leqslant (4-d)/8]$ is between that of the Edward-Willkinson model, $(2-d)/4$, and Mullins diffusion model, $(4-d)/8$. The local slope m is also a power law of time, $m \sim t^{n}$. The value of n for $2+1$ dimension shown in Fig. 2(b) is very small compared with the n for $1+1$ dimension shown in Fig. 2(a).

B. Schwoebel barrier effect

In this growth model, the step barrier (Schwoebel barrier) prevents adatoms to hop down the step edge, which generates an uphill diffusion current.[3,5,11] There are two important features in this kind of growth: (i) The surface is consisted of regular mound structures, having a wavelength selection. During growth, mounds coarsen, and the average mound separation λ grows as a power law $\lambda \propto t^{\delta}$, with δ ranging from 0.16 to 0.26;[5,11] (ii) the slope of mounds remains essentially constant after an initial transient, known as the slope selection. The selected slope is usually very small (less than 1.0).[3,5,11] This growth mechanism can be described by a nonlinear Langevin equation proposed by Johnson *et al.*[3]

$$\frac{\partial h(\mathbf{r},t)}{\partial t} = -\nu \nabla \frac{\nabla h}{1+(\nabla h)^2} - \kappa \nabla^4 h + \eta(\mathbf{r},t), \qquad (10)$$

where both ν and κ are positive. The first term on the right-hand side represents the uphill growth due to the Schwoebel barrier effect, and the second term is due to the surface diffusion (capillary effect). The up/down symmetry is still preserved for this equation although it is nonlinear. At the initial stage, as $|\nabla h|$ is small, Eq. (10) can be expanded as

$$\frac{\partial h(\mathbf{r},t)}{\partial t} = -\nu \nabla^2 h - \kappa \nabla^4 h + \eta(\mathbf{r},t). \qquad (11)$$

And $h(\mathbf{r},t)$ is a random Gaussian process.

Equation (11) actually looks very similar to Eq. (2) for the noise-induced rough surface except that the first term on the right-hand side has a negative coefficient, which implies that the solution for Eq. (11) is unstable. The coefficient ν here refers to the adatom diffuse process (the Schwoebel barrier effect), whereas the same coefficient in Eq. (2) stands for the effect of surface tension, or the evaporation/condensation process. Despite the different physical origins of Eq. (2) and Eq. (11), the solutions for the power spectrum are similar, except the negative sign in front of ν,

$$P(\mathbf{q}) = 4D \frac{1-e^{-2(\kappa q^4 - \nu q^2)t}}{\kappa q^4 - \nu q^2}. \qquad (12)$$

Equation (12) always has a maximum at $q_0 = \sqrt{(\nu/2\kappa)}$, which implies that the power spectrum $P(\mathbf{q})$ has a ring structure (in the $2+1$ dimension), and the peak position of the ring q_0 reflects the wavelength selection (average mound separation) $\lambda = 2\pi/q_0$ of the growth mechanism as shown in Fig. 3. This ring structure is the main difference between the two mechanisms we discussed above.

It is also interesting to note that the selected wavelength is only determined by the coefficients κ and ν, which correspond to the relative effect of surface diffusion and Schwoebel barrier. The ratio κ/ν plays a very important role for the growth mechanism. If $\kappa/\nu \gg 1$, which suggests that either Schwoebel barrier is small or surface diffusion is fast, the selected wavelength is too long for a technique (both real space imaging and diffraction techniques) to detect. In this case, the dominated roughening mechanism will still be the noise-induced dynamic roughening. In fact, as shown in Fig. 3(a), as the κ/ν ratio increases, the satellite ring intensity reduces and the ring radius shrinks. For a sufficiently large κ/ν (the curve for $\kappa/\nu = 20$ as shown in Fig. 3), one can hardly tell whether there exists a satellite ring or not. In this case only the capillary effect dominates, and the growth mechanism should be governed by Mullins diffusion, which gives $\beta = 0.25$.

Figure 3(b) shows a semilogarithmic plot of the time evolution of a power spectrum for selected κ/ν ratios. For a

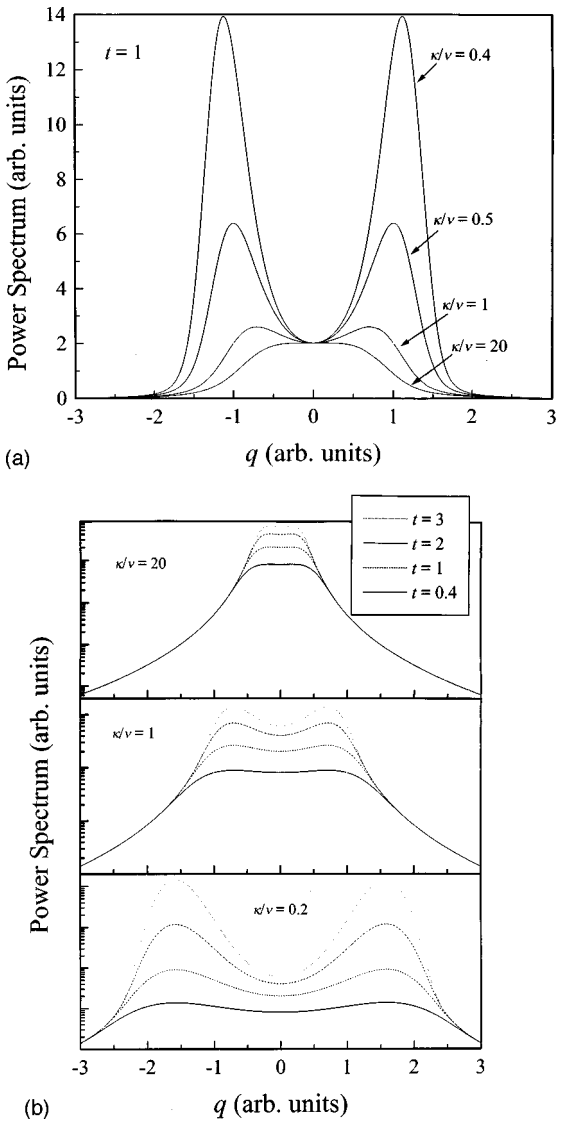

FIG. 3. The power spectrum of the zeroth-order solution for growth front roughening caused by Schwoebel barrier. (a) κ/ν ratio-dependent for $t=1$; (b) time-dependent for $\kappa/\nu=20$, 1, and 0.2.

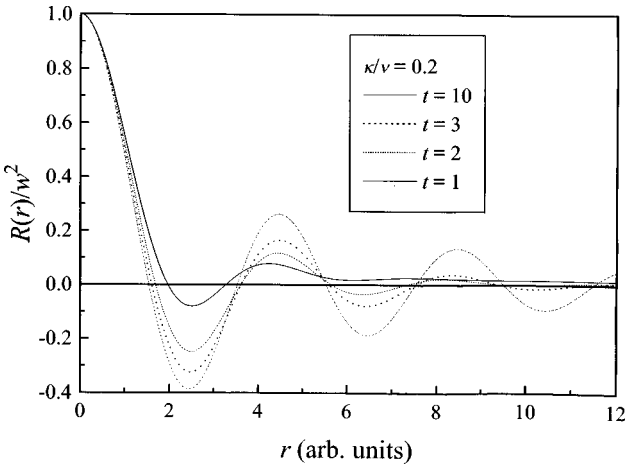

FIG. 4. The autocorrelation functions normalized by w^2 for $\kappa/\nu=0.2$ at different growth times. Note that the first zero crossing positions are different for different times.

large κ/ν ratio ($=20$), and after a long time deposition ($t=3$), there is only a tiny ring appeared in the power spectrum, which may not be able to detect in an experiment. However, for a medium κ/ν ratio ($=1$, crossover region), at the very beginning, the ring structure is still not observable. But for a sufficient long time, a clear satellite ring would appear. For a small κ/ν ratio, which means the Schwoebel barrier dominates, even at the initial stage, the ring structure is obvious in the power spectrum. Another interesting point is that the FWHM of the satellite ring (or the power spectrum for large κ/ν ratio) is a function of both the time t and ratio κ/ν. As the growth time becomes longer, the satellite ring becomes more obvious and sharper, which means that the

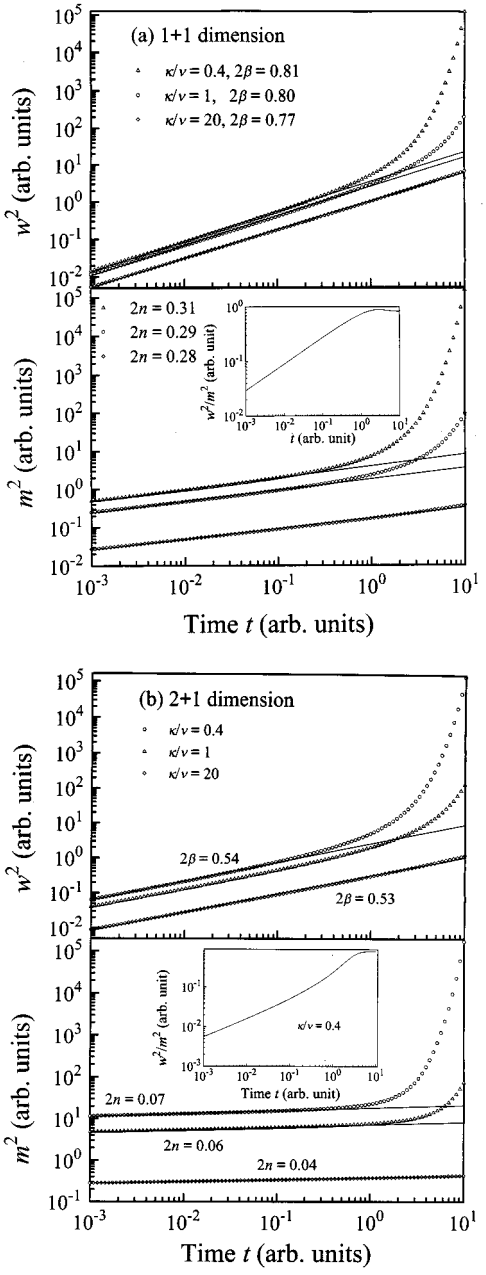

FIG. 5. Time evolution of the interface width w^2 and local slope m^2 of the zero-order solution for Schwoebel barrier induced growth front roughening: (a) $1+1$ dimension and (b) $2+1$ dimension. The insets are the plots of w^2/m^2 vs growth time t.

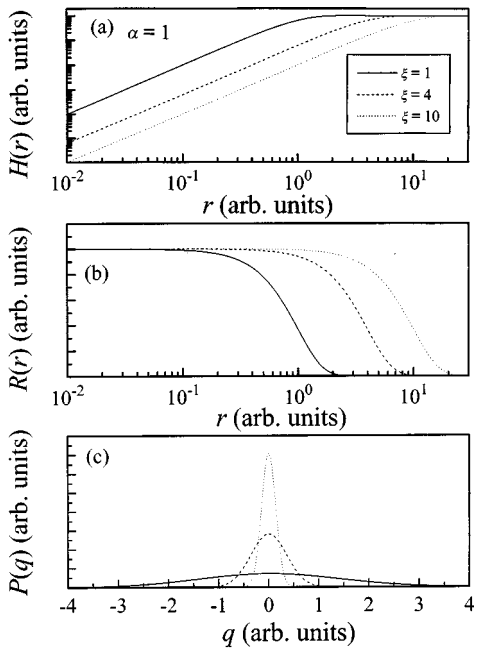

FIG. 6. Characteristic functions for self-affine surfaces in $2+1$ dimension: (a) height-height correlation function $H(r)$; (b) autocorrelation function $R(r)$; and (c) power spectrum $P(q)$.

local surface height fluctuation becomes more correlated (correlation length increases). Only when the local height fluctuation has a correlation length compatible to or larger than the average mound separation, can mounds dominate the morphology of the surface. This suggests that in order to describe a mound surface, one needs at least two relatively independent lateral lengths, one for describing the wavelength selection, and the other for describing the local roughness correlation. The relative weighting of these two lateral length scales determines the final morphology of the surface. Details will be presented in Sec. III.

Another point worth mentioning is that the location of the first zero crossing in the autocorrelation function is usually used as a measure of the average mound separation.[9,11,13] However, this is not entirely accurate. Figure 4 shows the autocorrelation functions for $\kappa/\nu = 0.2$ at different growth times. From the discussion above, the average mound separation λ is determined only by the κ/ν ratio, and different times should give the same mound separation value. However, as shown in Fig. 4, the autocorrelation functions at different times have different zero crossing positions, i.e., the shorter the growth time, the longer the first zero position. This is due to the effect of a competition between the two lateral lengths. Therefore, for a realistic growth system, both lateral lengths could change with the growth time, and the use of the first zero crossing position in the autocorrelation function as a sole measure of the average mound separation may be misleading.

For surfaces in both $1+1$ and $2+1$ dimensions, at the initial stage of growth the interface width w would grow as a power law of time t, $w \propto t^{\beta}$, with $\beta > \frac{3}{8}$ for $1+1$ dimension, and with $\beta > \frac{1}{4}$ for $2+1$ dimension (Fig. 5). For a longer time, w increases exponentially with t, and the unstable Laplacian term dominates the growth [which may not satisfy the small slope approximation assumed for Eq. (11), and the nonlinearity of Eq. (10) should be included]. The local slope m has a similar behavior, i.e., $m \propto t^{n}$ at initial stage, and $m \propto e^{ct}$ for longer times. As the κ/ν ratio is fixed, the average mound separation λ is also fixed. However, at the initial stage the power n is much less than β, which suggests that local slope m is not inversely proportional to the average mound separation λ. We plot the w^2/m^2 ratio vs growth time t as the inset for $\kappa/\nu = 0.4$. Only for longer growth times, the w^2/m^2 ratio reaches a constant. We conclude again that the average mound separation λ is not the only lateral parameter that determines the morphology of the growth front. We will demonstrate this later in our simple model in Sec. III.

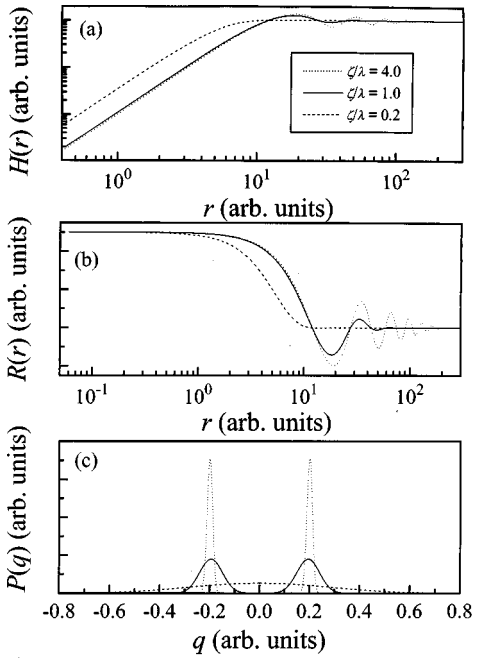

FIG. 7. Characteristic functions for mound surfaces in $2+1$ dimension: (a) height-height correlation function $H(r)$; (b) autocorrelation function $R(r)$; and (c) power spectrum $P(q)$.

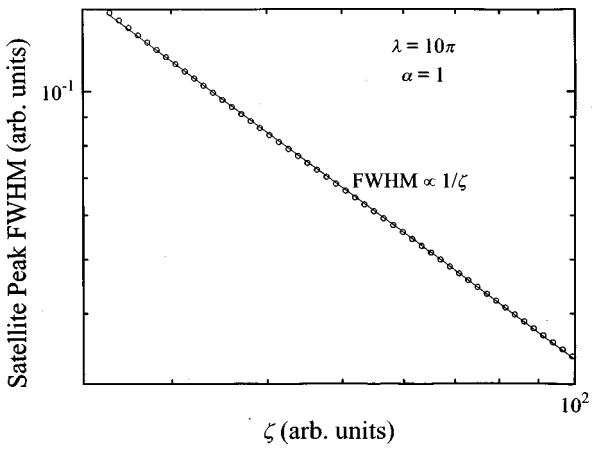

FIG. 8. The FWHM of the satellite peak is plotted as a function of system correlation length ζ for $2+1$ dimension.

III. GENERAL CHARACTERISTIC FUNCTIONS

In Sec. II we compare the power spectra between two different surface roughening mechanisms: the Schwoebel barrier effect and the noise-induced roughening. The main difference is that there is a characteristic ring structure in the power spectrum of a mound surface, while for a self-affine surface there is no ring structure. In order to use diffraction technique to differentiate these two kinds of surfaces, especially for a sufficiently large interface width, we need to know the characteristic function of the surface [height-height correlation function $H(\mathbf{r})$, or autocorrelation function $R(\mathbf{r})$, or power spectrum $P(\mathbf{q})$]. As demonstrated above, in some special cases the Langevin equations can be used to describe the surface growth and can be solved analytically. However, there are other models that cannot be solved analytically[3,8,9,13] but can be solved numerically.

In general, for noise-induced growth models, the height-height correlation function can be written as:[4] $H(\mathbf{r},t)=2w^2(t)f(r/\xi)$, where the scaling function $f(x)=1$ for $x\gg 1$, and $f(x)=x^{2\alpha}$ for $x\ll 1$. In this formula, $w\sim t^{\beta}$ is the interface width, ξ is the lateral correlation length, and α is the roughness exponent describing how wiggly the local surface is. The value of α ranges from 0 to 1.

In order to clearly illustrate the physics in the diffraction, we shall use phenomenological models to characterize the height-height correlation functions for different surfaces.

A. Height-height correlation $H(\mathbf{r})$ for noise-induced growth fronts

For a self-affine and isotropic surface, we use the height-height correlation function $H(r)$ proposed by Sinha and co-workers[12]

$$H(r)=2w^2[1-e^{-(r/\xi)^{2\alpha}}]. \tag{13}$$

Three parameters are used to describe the morphology of the surface, i.e., interface width w, lateral correlation length ξ, and roughness exponent α. This function works for both the $1+1$ dimension and the $2+1$ dimension, and is well known for describing self-affine surfaces. The corresponding autocorrelation function $R(r)$ is given by

$$R(r)=w^2e^{-(r/\xi)^{2\alpha}}. \tag{14}$$

When $\alpha=1$, the $1+1$ dimensional surface can be considered as a linear system with an independent Gaussian noise input $\eta(t)$. The system response function $Y(t)$ is a Gaussian function with a correlation length ξ. This correlation length determines the lateral correlation length of the output. The output signal is a convolution of $Y(t)$ and $\eta(t)$, i.e., $\int Y(\tau)\eta(t-\tau)d\tau$. The corresponding power spectrum takes the following form:

$$P(q)=\frac{w^2\xi}{\sqrt{2}}e^{-q^2\xi^2/4}. \tag{15}$$

In Fig. 6 we plot some examples of these characteristic functions with $\alpha=1$. It is clear to see that for a self-affine surface, both the height-height correlation function $H(r)$ and autocorrelation function $R(r)$ do not have an oscillatory behavior along the r axis, which captures the behavior of noise-induced surfaces discussed in Sec. II. The power spectrum has only a single peak at the center, and the FWHM of the peak is inversely proportional to the lateral correlation length ξ. The local slope for this kind of surface is determined by (only applied to $\alpha=1$ case)[10]

$$m^2=\langle(\nabla h)^2\rangle = \begin{cases} -\left.\dfrac{d^2R(r)}{dr^2}\right|_{r=0}=2\dfrac{w^2}{\xi^2} & \text{for } 1+1 \text{ dimension} \\ -2\left.\dfrac{\partial^2R(r)}{\partial x^2}\right|_{r=0}=4\dfrac{w^2}{\xi^2} & \text{for } 2+1 \text{ dimension,} \end{cases} \tag{16}$$

i.e., the local slope is only determined by the interface width w and lateral correlation length ξ. (Note that the average slope $\langle\nabla h\rangle$ is zero.)

B. Height-height correlation $H(\mathbf{r})$ for mound surfaces

For a mound surface, we propose the following form for the height-height correlation function:

$$H(r)=\begin{cases} 2w^2\left[1-e^{-(r/\zeta)^{2\alpha}}\cos\left(\dfrac{2\pi r}{\lambda}\right)\right] & \text{for } 1+1 \text{ dimension} \\ 2w^2\left[1-e^{-(r/\zeta)^{2\alpha}}J_0\left(\dfrac{2\pi r}{\lambda}\right)\right] & \text{for } 2+1 \text{ dimension,} \end{cases} \tag{17}$$

where $J_0(x)$ is the zeroth-order Bessel function. Four parameters are used to describe the surface, i.e., interface width w, system correlation length ζ, roughness exponent α, and average mound separation λ. For a mound surface it is known that the local slope is quite smooth and $\alpha=1$.[3,5,11] The corresponding autocorrelation functions are

$$R(r)=\begin{cases} w^2e^{-(r/\zeta)^{2\alpha}}\cos\left(\dfrac{2\pi r}{\lambda}\right) & \text{for } 1+1 \text{ dimension} \\ w^2e^{-(r/\zeta)^{2\alpha}}J_0\left(\dfrac{2\pi r}{\lambda}\right) & \text{for } 2+1 \text{ dimension.} \end{cases} \tag{18}$$

The lateral correlation length ξ can be defined through the autocorrelation function as $R(\xi)=w^2/e$, and is a function of both ζ and λ. For example, in the $2+1$ dimension, let $\zeta=\lambda$, then $\xi=0.27\lambda$. In fact, for the case of the $1+1$ dimension, the surface can also be considered as a linear system with the input as a product of an independent Gaussian noise $\eta(t)$ and a sinusoidal function $\sin(2\pi t/\lambda)$. The output signal is $\int Y(t-\tau)\sin[(2\pi/\lambda)\tau]\eta(\tau)d\tau$, where the response of the system $Y(t)$ is a Gaussian function with a system correlation length ζ. In fact, the system correlation length ζ determines how randomly the mounds are distributed on the surface. The smaller the ζ, the more random the distribution.

The corresponding power spectra are given by

$$P(q)=\begin{cases}\dfrac{w^2\zeta}{2\sqrt{2}}\left[e^{-(q-2\pi/\lambda)^2\zeta^2/4}+e^{-(q+2\pi/\lambda)^2\zeta^2/4}\right] & \text{for } 1+1 \text{ dimension} \quad (19a)\\ \dfrac{w^2\zeta^2}{2}\exp\left(-\dfrac{4\pi^2+q^2\lambda^2}{4\lambda^2}\zeta^2\right)I_0\left(\dfrac{\pi q\zeta^2}{\lambda}\right) & \text{for } 2+1 \text{ dimension,} \quad (19b)\end{cases}$$

where $I_0(x)$ is the zeroth-order modifid Bessel function. The additional parameter, the average mound separation λ, makes the problem more complicated. In Fig. 7 we plot the characteristic functions for various ζ/λ ratios in the $2+1$ dimension. The behavior of the characteristic functions is determined mainly by the ζ/λ ratio. If $\zeta/\lambda\geqslant 1$, both the height-height correlation function $H(r)$ and the autocorrelation function $R(r)$ have an oscillatory behavior, and the power spectrum shows a clear satellite ring. This is the essential characteristic of the rough surface caused by the Schwoebel barrier effect. In this case, the λ value gives the same satellite ring, located at $q_0=2\pi/\lambda$. The FWHM of the satellite ring decreases with the increasing system correlation length ζ for a fixed λ.

In fact, the FWHM of the satellite ring is inversely proportional to ζ as shown in Fig. 8. When the ζ/λ ratio is reduced, the oscillatory amplitude in both $H(r)$ and $R(r)$ decreases, and the ring position for the power spectrum also reduces even though λ remains unchanged. In Fig. 9 we show the change of the ring location as a function of the ζ/λ ratio. The solid curve represents $q_0=2\pi/\lambda$. Although the ring position is still inversely proportional to λ, the exact value is much different. As the ζ/λ ratio decreases further, the oscillatory behavior in both $H(r)$ and $R(r)$ totally disappears, and there is no longer a characteristic ring in the power spectrum.

The local slope can be calculated as

$$m^2=\begin{cases}2w^2\left(\dfrac{1}{\zeta^2}+\dfrac{2\pi^2}{\lambda^2}\right) & \text{for } 1+1 \text{ dimension}\\ 4w^2\left(\dfrac{1}{\zeta^2}+\dfrac{\pi^2}{\lambda^2}\right) & \text{for } 2+1 \text{ dimension.}\end{cases} \quad (20)$$

It is seen that the local slope is not only determined by the system correlation length ζ, but also by the average mound separation λ. When $\zeta/\lambda\gg 1$, $m^2\propto w^2/\lambda^2$, i.e., the local slope is determined only by the interface width w and average mound separation λ. However, as long as $\zeta/\lambda\ll 1$, then $m^2\propto w^2/\zeta^2$. The time-dependent behavior in Sec. II can be understood in terms of Eq. (20). Therefore, the above form of characteristic functions captures the essence of the rough surface we discussed in Sec. II, and also other published results from simulations and analytical work.[13]

IV. RECIPROCAL SPACE CHARACTERISTICS

One should keep in mind that the diffraction structure factor of a surface is not a simple Fourier transform of the surface morphology or the power spectrum. It is a Fourier transform of a more complicated function:[14]

$$S(\mathbf{q},t)=\int d^2r\ C(q_\perp,r)e^{i\mathbf{q}_\parallel\cdot\mathbf{r}}, \quad (21)$$

where $\mathbf{q}$ is the momentum transfer due to the diffraction, and can be decomposed into two orthogonal components, momentum transfer perpendicular to the surface $q_\perp$, and momentum transfer parallel to the surface, $\mathbf{q}_\parallel$. The height difference function $C(q_\perp,r)=\langle e^{iq_\perp[h(\mathbf{r},t)-h(0,t)]}\rangle$ has the form of

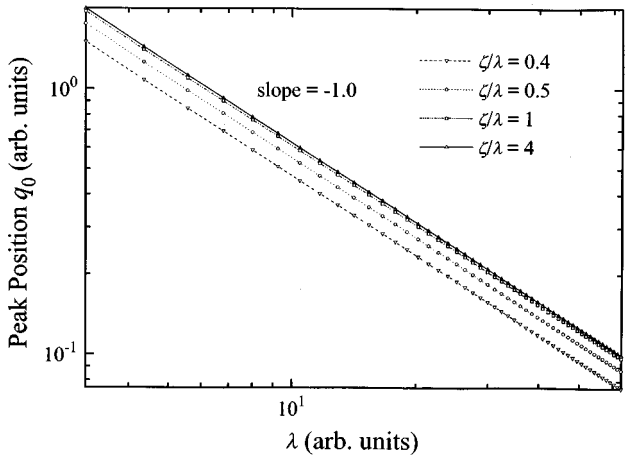

FIG. 9. The position of the satellite ring q_0 is plotted as a function of the average mound separation λ for different ζ/λ ratios for $2+1$ dimension. The solid curve is the plot of relation $q_0=2\pi/\lambda$.

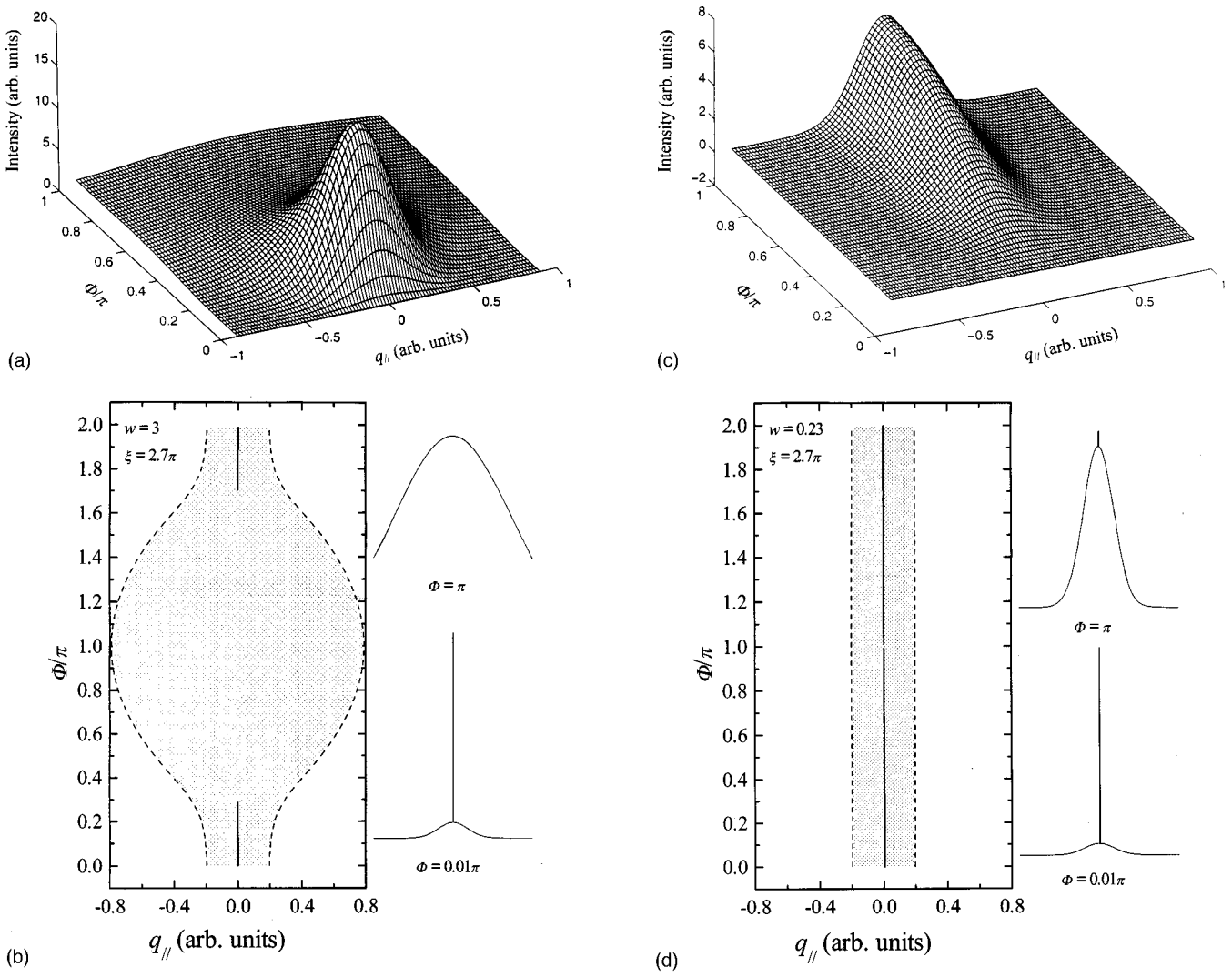

FIG. 10. Reciprocal space characteristics of the self-affine surfaces (2+1 dimension): (a) diffuse profiles for $w=3$ and $\xi=2.7\pi$ along the rod; (b) the diffraction structure factor for $w=3$ and $\xi=2.7\pi$; (c) diffuse profiles for $w=0.23$ and $\xi=2.7\pi$ along the rod; and (d) the diffraction structure factor for $w=0.23$ and $\xi=2.7\pi$. The shaded area between dotted curves in (b) and (d) represents the FWHM of the diffuse profile, and the central dark region refers to the δ peak and its relative intensity. The profiles on the right-hand side are selected diffraction profiles corresponding to $\Phi=0.01\pi$ (near in-phase) and $\Phi=\pi$ (out-of-phase).

$$C(q_\perp,r)\approx\frac{\sum_{N=-\infty}^{+\infty} e^{-(1/2)H(r,t)(\Phi-2n\pi)^2}}{\sum_{N=-\infty}^{+\infty} e^{-(1/2)H(r,t)(2n\pi)^2}}$$

for a Gaussian height distributed rough surface, and $C(q_\perp,r)=e^{-H(r,t)(1-\cos\Phi)}$ for a Poisson height distributed rough surface.[15] Here $\Phi=q_\perp c$, and c is the lattice constant. In this paper, we assume a Poisson height distribution (the use of a different height distribution does not alter the main conclusion of the present work).

A. Self-affine surfaces

The characteristics of the diffraction structure factor for the self-affine surface ($\alpha=1$, $\xi=2.7\pi$) along the reciprocal ''rod'' (cross section) are shown in Fig. 10 for both a large interface width $w=3$, and a small interface width $w=0.23$, respectively. The diffraction structure factors presented in Figs. 10(a) and 10(c) are only the diffuse profiles, and the complete rod structures are illustrated in Figs. 10(b) and 10(d), respectively. The shaded area between the dotted curves represents the FWHM of the diffuse profile, and the central dark region refers to the δ peak and its relative intensity. The δ peak reflects the long-range correlation of the surface height, and the diffuse profile is caused by the local roughness of the surface. The intensity of the δ peak decays as $e^{-2w^2(1-\cos\Phi)}$.

In the large interface width case ($w=3$), for the near in-phase condition where $\Phi\approx 2n\pi+\varepsilon$ ($n=0,\pm1,\pm2...$) and $|\varepsilon|\ll 1$, the diffraction structure factor contains a sharp central peak (theoretically a δ peak) and a broader diffuse profile as shown on the right panel in Fig. 10(b). At this condition, the inverse of the FWHM of the diffuse profile is a measure of the lateral correlation length ξ. However, the intensity of the diffuse profile is very small. The FWHM remains unchanged for small $|\varepsilon|$. As $|\varepsilon|$ increases, the intensity of the diffuse profile increases until it reaches a maximum at Φ

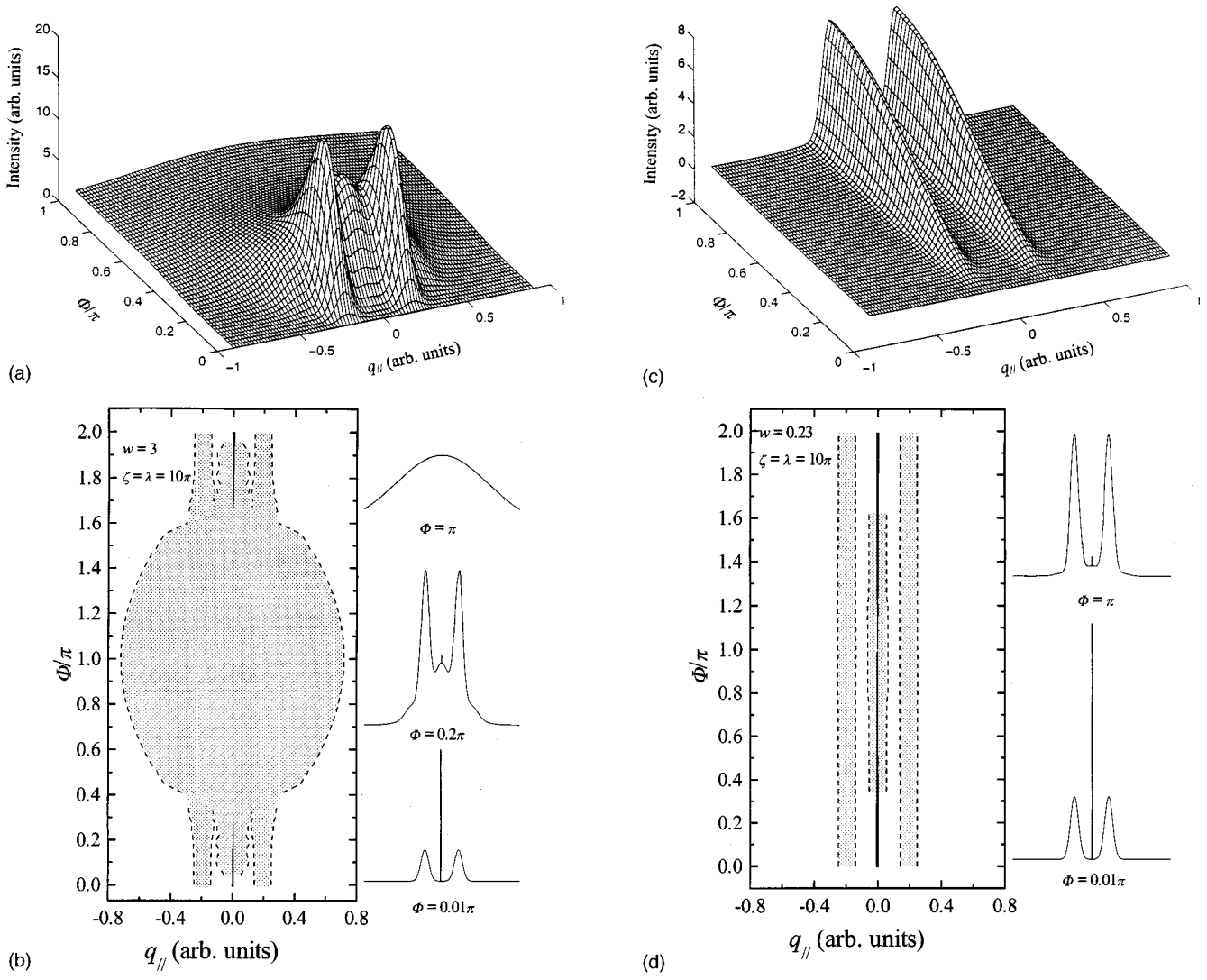

FIG. 11. Reciprocal space characteristics of the mound surfaces (2 + 1 dimension): (a) diffuse profiles for $w=3$ and $\zeta=\lambda=10\pi$ along the rod; (b) the diffraction structure factor for $w=3$ and $\zeta=\lambda=10\pi$; (c) diffuse profiles for $w=0.23$ and $\zeta=\lambda=10\pi$ along the rod; and (d) the diffraction structure factor for $w=0.23$ and $\zeta=\lambda=10\pi$. The shaded area between dotted curves in (b) and (d) represents the FWHM of the diffuse profiles and the central dark region refers to the δ peak and its relative intensity. The profiles on the right-hand side are the selected diffraction profiles corresponding to $\Phi=0.01\pi$ (near in-phase), $\Phi=0.2\pi$, and $\Phi=\pi$ (out-of-phase).

$\approx 0.4\pi$. Then the intensity of the diffuse profile begins to decrease, and its shape begins to broaden while the δ peak begins to diminish. In fact, this is the requirement of the conservation of energy, the total diffracted beam should equal the total incident beam. At the out-of-phase condition where $\Phi=2n\pi+\pi$, only the diffuse profile can be seen and its FWHM reaches the maximum value. At this condition the FWHM of the profile is a measure of the average local slope of the rough surface.[14]

In the small interface width case ($w=0.23$), for both the near in-phase condition and the out-of-phase condition, the diffraction structure factor always contains a sharp central peak (theoretically a δ peak) and a broader diffuse profile [Fig. 10(d)]. In this case, the FWHM of the diffuse profile along the rod is almost a constant, and actually is a measure of the lateral correlation length ξ. The intensity of the diffuse profile increases monotonically as $|\varepsilon|$ increases from near 0 to π. It is very clear that no splitting occurs along the rod for both large and small w cases.

B. Mound surfaces

The reciprocal space structure of the diffraction profile for this surface ($\alpha=1$, $\zeta=\lambda=10\pi$) is shown in Fig. 11 for both a large interface width $w=3$, and a small interface width $w=0.23$. In the large interface case, under the near in-phase condition ($|\varepsilon|\ll 1$), there is a central δ peak and a clear satellite ring around the δ peak [see the diffraction profile at $\Phi=0.01\pi$ in Fig. 11(b)]. This profile is quite different from the self-affine case shown in Fig. 10 where a broad central diffuse intensity exists in addition to the δ peak. The satellite peak position q_0 shown in Fig. 11 is a measure of the average mound separation λ, $\lambda\approx 2\pi/q_0$. With the increase of the phase ($|\varepsilon|$), a central diffuse intensity gradually appears with increasing intensity in addition to the δ peak, and the FWHM of the diffuse central intensity remains almost unchanged [see the diffraction profile at $\Phi=0.2\pi$ in Fig. 11(b)]. After reaching a maximum intensity ($\Phi\approx 0.2\pi$, depending on the roughness parameters w, ζ, and λ), the split satellite intensity

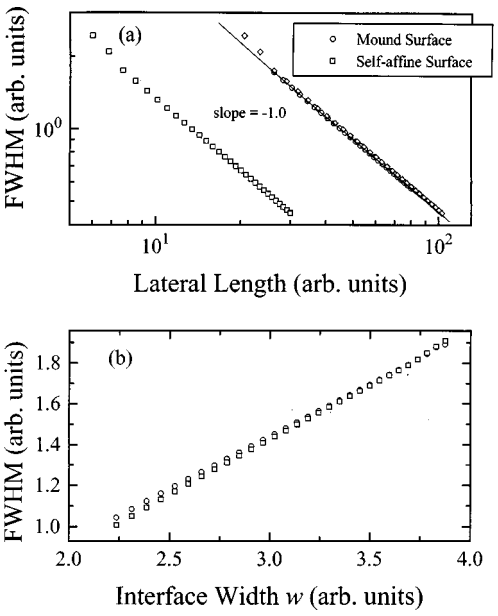

FIG. 12. A comparison of FWHM of the diffuse profile at the out-of-phase condition for different surfaces (2+1 dimension): (a) as a function of lateral length (ξ, squares for a self-affine surface; and λ ($=\zeta$), open circles for a mound surface). The diamonds superposed on the open circles represent FWHM's of a self-affine surface after the rescaling of the lateral correlation length ξ; and (b) as a function of the interface width w for a fixed ξ ($=0.27\lambda$) and λ ($=\zeta=10\pi$).

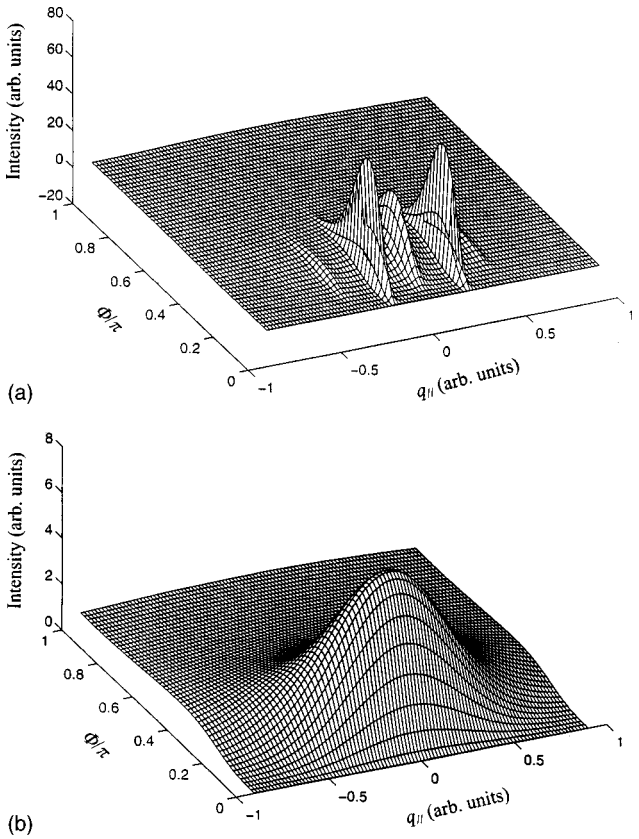

FIG. 13. Diffuse profiles along the rod for mound surfaces (2+1 dimension): (a) $w=3$ and $\zeta=4\lambda=40\pi$; (b) $w=3$ and $\zeta=0.2\lambda=2\pi$.

begins to decrease. The width of the central diffuse intensity continues to broaden. At $\Phi\approx 0.4\pi$ the satellite peak is buried in the broadened central intensity. At this point virtually one cannot tell the position of the satellite peak from the profile.

At the out-of-phase condition, the profile becomes one single broad peak very similar to that obtained from a self-affine rough surface [see the diffraction profile at $\Phi=\pi$ in Fig. 10(b)]. Figure 12 shows the FWHM as a function of interface width w and average mound separation λ (here $\zeta=\lambda$) as compared to that of a self-affine surface at the out-of phase condition. It is shown that FWHM$\propto w/\lambda$, i.e., the FWHM of this peak is still a measure of the average local slope or the average mound slope. However, the FWHM for both the mound surface and self-affine surface is overlapping on the same curve, which means that at the out-of-phase condition one cannot tell from the diffraction profile whether the surface has mounds or not. The reason that near the out-of-phase condition the profile is not sensitive to the wavelength selection, is that for a sufficiently large w the dominant contribution in Eq. (21) is from the small r regime due to the exponential factor in the $C(q_\perp,r)$. The oscillatory behavior in the height-height correlation is in the large r regime and its contribution becomes small in the exponential factor.

In the small interface width case ($w=0.23$), the diffraction profiles are much different from those of the large interface width case. The satellite ring and the δ peak can be seen throughout the whole rod [Fig. 11(d)]. The FWHM of the satellite ring remains almost the same, and is a reflection of the system correlation length [Fig. 11(d)]. The intensity of satellite ring increases monotonically as $|\varepsilon|$ increases from near 0 to π.

It is also interesting to show the relationship between the diffraction profiles and the ζ/λ ratio. In Fig. 13 we plot the diffraction profiles for different ζ/λ ratios in the large interface width case ($w=3$). Compared with Figs. 11(a) and 11(b), as the ζ/λ ratio increases, the satellite ring at the near in-phase condition is much narrower, and the center diffuse profile is well separated from the satellite ring. However, when the ζ/λ ratio is small [as shown in Fig. 13(b), $\zeta/\lambda=0.2$], even at the near in-phase condition, one cannot tell the position of the satellite ring, and the diffraction structure is much like that of a self-affine surface [for example, Fig. 10(a)]. This behavior of diffraction structure factor is similar to that of the power spectrum as shown in Fig. 7.

For a surface with Gaussian height distribution, some quantitative changes are necessary at the out-of-phase condition, but no change is required at the near in-phase condition or for the small interface width case.[14,15]

V. DISCUSSION AND CONCLUSION

It is seen from Sec. IV that the reciprocal space characteristics originated from the noise-induced surface or SB mound surface are quite different for either the small interface width case or the large interface width case at near the in-phase condition, but they are similar for the large interface width or at the out-of-phase condition. This can be understood from the following discussion.

The diffraction profile is determined by the Fourier transform of a height difference function $C(q_\perp,r)$ in Eq. (21).

For a Poisson height distribution, $C(q_\perp,r)$ can be rewritten as

$$C(q_\perp,r)=e^{-\Omega f(r)}, \tag{22}$$

where $\Omega=2w^2(1-\cos\Phi)$ and $f(r)=H(r)/2w^2$. We have $0\leqslant f(r)\leqslant a$, where $a=1$ for a self-affine surface and $1\leqslant a<2$ for a mound surface. This means that the value of Ω determines the asymptotic behavior of $C(q_\perp,r)$, and therefore the behavior of the diffraction profile. Combining Eq. (22) with Eq. (21), in general, the diffraction profile can be written as[14]

$$S(\mathbf{q}_\parallel,\Omega)=\int e^{-\Omega f(r)}e^{i\mathbf{q}_\parallel\cdot\mathbf{r}}d\mathbf{r}. \tag{23}$$

It can be broken into two parts

$$S(\mathbf{q}_\parallel,\Omega)=S_\delta(\mathbf{q}_\parallel,\Omega)+S_{\rm diff}(\mathbf{q}_\parallel,\Omega), \tag{24}$$

where

$$\begin{aligned}S_\delta(\mathbf{q}_\parallel,\Omega)&=\int C(q_\perp,r\to\infty)e^{i\mathbf{q}_\parallel\cdot\mathbf{r}}d\mathbf{r}\\&=(2\pi)^dC(q_\perp,r\to\infty)\,\delta(\mathbf{q}_\parallel),\end{aligned} \tag{25}$$

$$S_{\rm diff}(\mathbf{q}_\parallel,\Omega)=\int[C(q_\perp,r)-C(q_\perp,r\to\infty)]e^{i\mathbf{q}_\parallel\cdot\mathbf{r}}d\mathbf{r}, \tag{26}$$

here d stands for the dimension, $d=1$ for $1+1$ dimension, and $d=2$ for $2+1$ dimension. For both a self-affine surface and a mound surface, we have

$$C(q_\perp,r\to\infty)=e^{-\Omega}. \tag{27}$$

Therefore the intensity ratio of the δ peak to the total integrated intensity can be calculated as

$$R_\delta=\frac{\int\int S_\delta(\mathbf{q}_\parallel,\Omega)d\mathbf{q}_\parallel}{\int\int S(\mathbf{q}_\parallel,\Omega)d\mathbf{q}_\parallel}\propto e^{-\Omega}=e^{-2w^2(1-\cos\Phi)}. \tag{28}$$

That is, the interface width can be determined through the intensity ratio R_δ, for both a self-affine surface and a mound surface.

The diffuse profile can be written as

$$S_{\rm diff}(\mathbf{q}_\parallel,\Omega)=e^{-\Omega}\int(e^{\Omega[1-f(r)]}-1)e^{i\mathbf{q}_\parallel\cdot\mathbf{r}}d\mathbf{r}. \tag{29}$$

For $\Omega\ll 1$, we can expand the integral kernel in Eq. (29) into a power series and only the first term will contribute significantly in the integral, i.e.,

$$S_{\rm diff}(\mathbf{q}_\parallel,\Omega)=2(2\pi)^d(1-\cos\Phi)P(\mathbf{q}_\parallel). \tag{30}$$

Equation (30) does not depend on the specific surface morphology as long as the condition $\Omega\ll 1$ is satisfied. Therefore, at the near in-phase condition or for a small interface width, where $2w^2(1-\cos\Phi)\ll 1$, the diffraction structure factor without the δ peak is actually identical to the power spectrum $P(\mathbf{q},t)$, of a rough surface. For a self-affine surface with $\alpha=1$, the power spectrum has the form of a Gaussian function [Eq. (15)] with the center at $q_0=0$. The FWHM of this diffuse profile is inversely proportional to the lateral correlation length ξ, FWHM $\sim 1/\xi$. However, for a mound surface, the power spectrum has the form of Eq. 19(b). Unlike the power spectrum of a self-affine surface, it has a peak located at $q_0\approx 2\pi/\lambda$ $(\zeta\gg\lambda)$, which is a reflection of the wavelength selection. This would provide a definitive way to differentiate the two mechanisms in a growth front. Also the FWHM of the peak is inversely proportional to the system correlation length ζ.

When Ω increases, the higher order expansions in Eq. (29) will take effect. The picture will be clearer if we consider the $1+1$ dimension case as an example. For the $1+1$ dimension, Eq. (29) becomes

$$\begin{aligned}S_{\rm diff}(q_\parallel,\Omega)&=e^{-\Omega}\int\sum_{n=1}^{\infty}\frac{\Omega^n}{n!}[1-f(r)]^ne^{iq_\parallel r}dr\\&=e^{-\Omega}\sum_{n=1}^{\infty}\frac{2^n(1-\cos\Phi)^n}{n!}\\&\quad\times\underbrace{P(q_\parallel)*P(q_\parallel)*\cdots*P(q_\parallel)}_{n},\end{aligned} \tag{31}$$

i.e., $S_{\rm diff}(\mathbf{q}_\parallel,\Omega)$ will become the sum of a self-convolution of the power spectrum, and the contribution of higher-order terms to $S_{\rm diff}(\mathbf{q}_\parallel,\Omega)$ will become more important. The result of convolution is to distort the power spectrum and to broaden the whole profile. Therefore, for a self-affine surface, the FWHM of the diffuse profile tends to broaden. But for a mound surface, the splitted peaks will broaden and then merge together. The separation of the peaks will become less obvious. A similar behavior would be expected for the $2+1$ dimension although there is no simple convolution theorem that can be applied as in the $1+1$ dimension case.

For $\Omega\gg 1$, we can deduce an asymptotic behavior of the diffraction profile. Since $\Omega\gg 1$, $C(q_\perp,r)$ is clearly confined to the short-range regime. For a self-affine surface and $\alpha=1$, the short-range height difference function can be expressed as

$$C(q_\perp,r)\approx\exp\left(-\frac{\Omega r^2}{\xi^2}\right). \tag{32}$$

Then

$$S_{\rm diff}(\mathbf{q}_\parallel,\Omega)\approx\frac{2\pi\xi^2}{\Omega}\exp\left(-\frac{q_\parallel^2\xi^2}{4\Omega}\right). \tag{33}$$

It seems that Eq. (33) still preserves the form of the power spectrum. However, the argument for the Gaussian function is totally different. It depends not only on the lateral correlation length ξ, but also on Ω. The FWHM has the following relation

$$\text{FWHM}\propto\frac{\sqrt{\Omega}}{\xi}\propto\frac{w}{\xi}=m, \tag{34}$$

that is, under this condition, FWHM is determined by the local slope only.

For a mound surface, the short-range height difference function can be expressed as

$$C(q_\perp,r)\approx\exp\left[-\Omega r^2\left(\frac{1}{\zeta^2}+\frac{\pi^2}{\lambda^2}\right)\right]. \tag{35}$$

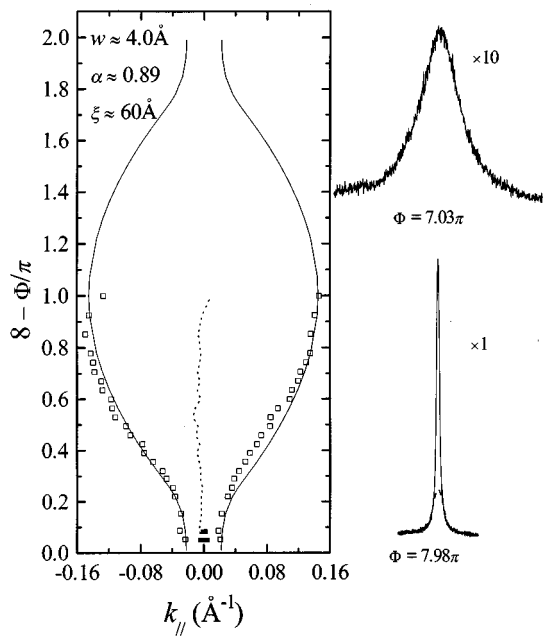

FIG. 14. The diffraction structure factor of the (00) beam measured from the Si/Si(111) surface grown at 275 °C at the later stage of growth. There is no split satellite peaks in all the measured profiles along the reciprocal rod. The profiles on the right correspond to $\Phi=7.98\pi$ (near in-phase) and $\Phi=7.03\pi$ (near out-of-phase). The δ peaks represented by the filled rectangles along the (00) rod exist at and near in-phase conditions. The δ peak intensity decreases rapidly when the diffraction condition moves away from the in-phase condition. The dotted curve represents the peak positions of the diffuse profiles. The open squares represent the FWHM of the diffuse profiles. The solid curves are fits using Eq. (21) with Eq. (13) as the height-height correlation function with the roughness parameters, $w\approx4.0$ Å, $\alpha\approx0.89$, and $\xi\approx60$ Å.

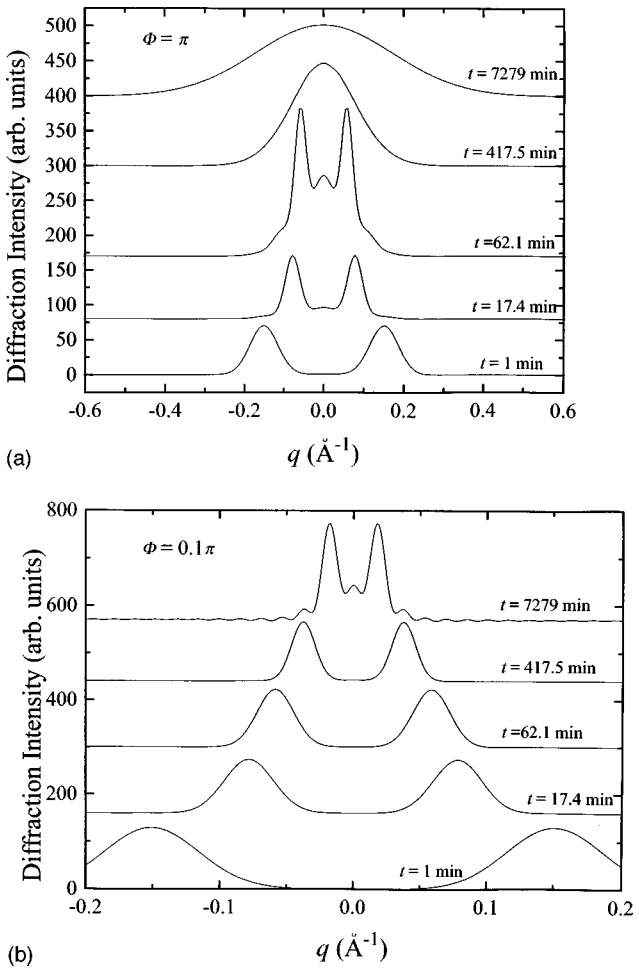

FIG. 15. Simulated HRLEED diffuse profiles for Cu/Cu(100) epitaxial growth: (a) out-of-phase condition ($\Phi=\pi$); and (b) near in-phase condition ($\Phi=0.1\pi$).

If we define $1/\xi'^2=1/\zeta^2+\pi^2/\lambda^2$, then the diffraction profile would have the same form as Eq. (33) by simply substituting ξ by ξ'. The diffraction profile becomes a simple Gaussian shape, and the characteristics of a power spectrum are totally lost. The FWHM has the relation

$$\mathrm{FWHM}\propto\frac{\sqrt{\Omega}}{\xi'}\propto w\left(\frac{1}{\zeta^2}+\frac{\pi^2}{\lambda^2}\right)^{1/2}=m, \tag{36}$$

that is, the FWHM is also determined by the local slope. For the SB growth mechanism, as the surface reaches its steady slope regime (slope selection), the shape of a diffraction profile at the out-of-phase condition should not change.

Therefore, for both self-affine and mound surfaces, if $\Omega\gg1$, which corresponds to a large interface width and near the out-of-phase diffraction condition, the diffraction profile has exactly the same form, and the FWHM of the profile is proportional to the local slope. One cannot differentiate these two surfaces at this condition.

At the out-of-phase diffraction condition, the diffraction profile is very sensitive to a small roughness change during the initial stage of growth.[8,9,11,16] However, as the interface width grows, only the characteristics of the local structure (such as the local slope) are reflected in the diffraction profile under this condition. For other quantitative information such as the interface width, the lateral correlation length, or the average mound separation, one has to measure the diffraction profiles at near in-phase condition.

To confirm the present analysis, we analyze the diffraction data of the rough growth front observed in our Si/Si(111) homoepitaxy experiment at the near in-phase diffraction condition. The growth was performed in a UHV chamber equipped with a high-resolution low-energy electron-diffraction (HRLEED) system with an instrument resolution of 6×10^{-3} Å^{-1} (FWHM). The growth was carried out at a temperature of 275 ± 5 °C for 10 min, with a rate of 8 ± 1 bilayer/min. The detailed experimentation can be found in Refs. 16 and 17. The HRLEED diffraction profiles were taken by varying the incident electron energy in order to span the reciprocal rod. Figure 14 shows a reciprocal rod structure at the deposition time $t=10$ min. The center dotted curve indicates the peak positions of the diffuse profiles. The fluctuation is due to uncertainties in the profile measurement and the fits of the decomposed diffuse profiles. The open squares are the positions of the half maximum of the diffuse profiles. The solid curves are fits using Eq. (21) with Eq. (13) as the height-height correlation function with the roughness parameters, $w\approx4.0$ Å, $\alpha\approx0.89$, and $\xi\approx60$ Å. This structure along the rod is similar to that shown in Fig. 10(b), and there is no splitting in the profiles along the rod at any deposition time. Therefore, this growth front is

consistent with the noise-induced roughening rather than the mound formation caused by the SB effect.[16]

For the mound formation systems such complete data is not available yet in the literature. Although a clear splitting in the diffraction profile near the in-phase condition has been observed from a quasiperiodic facetted surface by Falta and co-workers,[18] the reciprocal space structure is totally different: the splitting increases as one goes from the near in-phase condition to the out-of-phase condition. But for the mound surface the splitting remains the same or even merges together near the out-of-phase condition. The splitting in the facetting surface does not directly reflect the periodicity of the surface, while the splitting in the mound surface gives the average mound separation. Here, we simulate the HRLEED profiles of Cu/Cu(100) growth by using our proposed model and the time-dependent interface width and mound separation data from Ref. 11. In Fig. 15 we plot the time evolution of the HRLEED profiles at both the out-of-phase ($\Phi=\pi$) and in-phase ($\Phi=0.1\pi$) conditions. At the out-of-phase condition, both simulated profiles and experimental data[11] show that a satellite structure exists at the initial stages of growth. When the epitaxial layer reaches 100 ML and higher, experimental data showed that the diffraction beam became one single broad profile, and no satellite ring was observed. This is also described by our simulations [the profile at $t=417.5$ min and $t=7279$ min in Fig. 15(a)]. However, at the near in-phase condition, although there was no experimental data, the simulated diffraction profile as a function of time always has the satellite ring, and the diameter of the ring keeps on shrinking, which reflects the coarsening of the mounds. This is where much quantitative information could be obtained if data were available.

In conclusion, we compared the characteristic functions of the self-affine rough surfaces and mound surfaces. Phenomenological characteristic functions are used to describe the difference. We show that if one moves away from the out-of-phase diffraction condition, the general reciprocal space structure obtained from a self-affine rough surface is dramatically different from that obtained from a rough surface caused by the SB effect. This provides a possible way to differentiate surface growth morphology induced by these two mechanisms using diffraction techniques.

ACKNOWLEDGMENTS

This work was supported by NSF No. DMR-9531482. We thank J. B. Wedding for reading the manuscript.

[1] F. Rosenberger, in *Interfacial Aspects of Phase Transformations*, edited by B. Mutaftschiev (Reidel, Dordrecht, 1982), pp. 315–364; R. Kunkel, B. Poelsema, L. K. Verheij, and G. Comsa, Phys. Rev. Lett. **65**, 733 (1990).

[2] For a review, see T. Halpin-Healy and Y.-C. Zhang, Phys. Rep. **254**, 215 (1995).

[3] J. Villian, J. Phys. I (France) **1**, 19 (1991); M. D. Johnson, C. Orme, A. W. Hunt, D. Graff, J. Sudijono, L. M. Sander, and B. G. Orr, Phys. Rev. Lett. **72**, 116 (1994); M. Siegert and M. Plischke, *ibid.* **73**, 1517 (1994).

[4] For a review, see *Dynamics of Fractal Surfaces*, edited by F. Family and T. Vicsek (World Scientific, Singapore, 1990); A.-L. Barabási and H. E. Stanley, *Fractal Concepts in Surface Growth* (Cambridge University Press, New York, 1995).

[5] P. E. Hegeman, H. J. W. Zandvliet, G. A. M. Kip, and A. van Silfhout, Surf. Sci. **311**, L655 (1994); J. A. Stroscio, D. T. Pierce, M. D. Stiles, A. Zangwill, and L. M. Sander, Phys. Rev. Lett. **75**, 4246 (1995); J. E. Van Nostrand, S. J. Chey, M.-A. Hasan, D. G. Cahill, and J. E. Greene, *ibid.* **74**, 1127 (1995); F. Tsui, J. Wellman, C. Uher, and R. Clarke, *ibid.* **76**, 3164 (1996).

[6] H.-N. Yang, G.-C. Wang, and T.-M. Lu, *Diffraction from Rough Surfaces and Dynamic Growth Fronts* (World Scientific, Singapore, 1993).

[7] H.-N. Yang, T.-M. Lu, and G.-C. Wang, Phys. Rev. Lett. **68**, 2612 (1992).

[8] M. C. Bartelt and J. W. Evans, Phys. Rev. Lett. **75**, 4250 (1995); Langmuir **12**, 217 (1996).

[9] J. G. Amar and F. Family, Surf. Sci. **365**, 177 (1996).

[10] T. Assefi, *Stochastic Processes and Estimation Theory with Application* (Wiley, New York, 1979).

[11] J.-K. Zuo and J. F. Wendelken, Phys. Rev. Lett. **78**, 2791 (1997).

[12] S. K. Sinha, E. B. Sirota, and S. Garoff, Phys. Rev. B **38**, 2297 (1988).

[13] Pavel Smilauer and Dimitri D. Vvedensky, Phys. Rev. B **52**, 14 263 (1995); Martin Siegert and Michael Plischke, Phys. Rev. E **53**, 307 (1996); M. Rost and J. Krug, *ibid.* **55**, 3952 (1997).

[14] H.-N. Yang, G.-C. Wang, and T.-M. Lu, *Diffraction from Rough Surfaces and Dynamic Growth Fronts* (Ref. 6), Chap. III, p. 82–135; Phys. Rev. B **47**, 3911 (1993).

[15] Y.-P. Zhao, G.-C. Wang, and T.-M. Lu, Phys. Rev. B **55**, 13 938 (1997).

[16] H.-N. Yang, G.-C. Wang, and T.-M. Lu, Phys. Rev. Lett. **73**, 2348 (1994).

[17] H.-N. Yang, G.-C. Wang, and T.-M. Lu, Phys. Rev. Lett. **74**, 2276 (1995). The film prepared in Ref. 16 before the annealing was used for data collection and analysis in this letter.

[18] J. Falta, R. Imbihl, and M. Henzler, Phys. Rev. Lett. **64**, 1409 (1990). In fact the surface morphology observed in their diffraction experiment is from a quasiperiodic facetting surface. The splitting at the near-in-phase condition is due to the (00) beams from the (340) and (430) facets.